Heliyon 9 (2023) e17809

Contents lists available at ScienceDirect

Heliyon

journal homepage: www.cell.com/heliyon

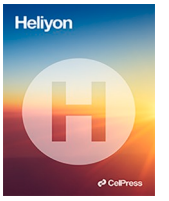

X-ray diffraction studies of a partially demineralized oriented cortical bone with the controlled depth of analysis

Sergei Danilchenko [a], Aleksei Kalinkevich [a,*], Mykhailo Zhovner [a], He Li [b], Aleksandr Kochenko [a], Petro Danylchenko [c], Jufang Wang [b]

[a] Institute of Applied Physics, NASU, 58 Petropavlivska St., 40000, Sumy, Ukraine
[b] Institute of Modern Physics, Chinese Academy of Sciences, 509 Nanchang Rd., Lanzhou, 730000, China
[c] Institute of Physics, Faculty of Science, P.J. Šafárik University, 9, Park Angelinum, 04154, Košice, Slovak Republic

ARTICLE INFO

Keywords:
Bone tissue
Demineralization
Bioapatite
Crystal microstructure
X-ray diffraction

ABSTRACT

The *in vitro* demineralization of bone tissue is used for simulating the osteoporosis related bone loss. This way would be helpful in observations of bone apatite dissolution in microstructural level and may give significant input for understanding crystal-chemistry of bone resorption. In the case of cortical bone, demineralization occurs inhomogeneously, with the formation of a superficial demineralized layer and a transition zone with a gradient of concentration and structural characteristics perpendicular to the reaction advance front. Changes in the microstructural parameters of the bone mineral in this interface zone are of great interest for understanding the resorptive processes in the bone associated with osteoporosis. In this work, the SEM-EDX method was used to estimate the sizes of the demineralized and interface layers in the cortical bone during stepwise demineralization in HCl water solution; the general patterns of changes in the concentrations of Ca, P, and Cl in these layers were established. The calculations of the effective penetration depth of X-rays in diffraction mode for the intact and partially demineralized cortical bone were performed. It is shown that the use of CoKα radiation (instead of the usual CuKα) ensures the depth of probing within the interface zone, which allows to adequately assess the microstructural parameters (crystallite sizes and lattice microdeformations) of altered bioapatite in the zone of its interaction with an acid agent. A nonmonotonic change in the average size of crystallites and microdeformations of the apatite lattice was revealed during acid demineralization of the bone. Using asymmetric XRD geometry, the evidence was obtained that the affected mineral of the transition zone does not contain other crystalline phases except for weakly crystallized apatite. For the first time, the depth-controlled XRD analysis was applied to such a complex (surface-gradient) object as partially demineralized cortical bone. Additionally, we propose a rapid, averaging, and non-destructive method for estimating the depth of the reaction front dividing the demineralized and non-demineralized portions of the bone by XRD. The consistency of XRD and SEM-EDX data on the thickness values of the demineralized layer is shown.

1. Introduction

The *in vitro* demineralization of bone tissue attracts interest because in a living organism bone mineral normally dissolves during

* Corresponding author.
E-mail address: kalinkevich@ipflab.sumy.ua (A. Kalinkevich).

https://doi.org/10.1016/j.heliyon.2023.e17809
Received 17 March 2023; Received in revised form 27 June 2023; Accepted 28 June 2023
Available online 29 June 2023

lifetime. Ongoing changes to bone tissue are made possible by specialized cells called osteoclasts, which break down old bone, and osteoblasts, which build new bone. This continuous process allows the bone to adapt and maintain its structure. However, when there is an imbalance between these two types of cells, it can lead to serious bone conditions like osteoporosis [1–3]. Osteoporosis causes a significant reduction in bone mineral density and affects the mineral properties, which leads to the increase of fracture risk and skeletal deformity [4,5]. The analogous affects occur under such negative external factors as prolonged weightlessness and immobilization of biological objects [6,7]. That is why the immobilization of biological objects is often used for study the osteoporosis related bone loss [8,9]. However, experiments with living models are very expensive, time consuming and are not irreproachable in terms of the ethics of laboratory animals handling (even subjecting to extensive ethical procedures). Thus, strategies for replacing living animal experiments are favored more and more in biological and medical research. It seems very promising to develop an *in vitro* method to decrease mineral content of devitalized bone by chemical agents that alters the bone mineral to simulate osteoporosis. This also would be helpful in observations of bone apatite dissolution in microstructural level and may give significant input for understanding crystal chemistry of bone resorption.

Currently, there is limited research focused on using chemical agents to reduce the mineral content of animal bones in a laboratory setting. These agents can change the density of the bone minerals and certain biomechanical properties to create a simulation of osteoporosis in humans [10–12]. Some authors imply that the acid demi + neralizing process may be useful for producing a vertebra that has some biomechanical properties that are characteristic for osteoporosis. However, a uniform decrease in the mineral density of compact or cortical bone is a difficult and hardly feasible task.

In the process of dissolution of the cortical bone mineral the formation of a growing demineralized layer on the bone surface takes place, and the reaction front advances into the tissue with increasing immersion time of bone block in the decalcifying agent [13–15]. Moreover, while Lewandrowski et al. [13] and Horneman et al. [14], with some stipulations, reported on the two-zone structure (demineralized and mineralized matrix) of the transverse section of the bone after acid treatment, in Ref. [15], in addition to these two, a third interface zone or contact zone was noted and characterized by SEM and EDX. In Ref. [13], the authors discuss the presence of an interface, measuring 20 μm in thickness, between the demineralized and non-demineralized sections of the bone at the reaction front. However, it is not mentioned whether this interface remains consistent or undergoes any changes in response to variations in acid concentration or the duration of immersion. In the study [15], the researchers discovered a distinct region, referred to as the interface, which exhibited unique characteristics. The properties of this interface, such as the calcium-to-phosphorus ratio ranging from 1.4 to 1.5 and a thickness spanning between 16 and 43 μm, were found to be influenced by factors like acid concentration, duration of acid exposure, and specific anatomical regions. Understanding the alterations occurring in the microstructural parameters of the bone's apatite within this interface zone holds significant importance in comprehending the resorption processes associated with osteoporosis.

Several studies using XRD have monitored the change in the structural characteristics of the cortical bone mineral during demineralization [e.g., 16, 17], but the samples were reduced to powder form before analysis, which averaged the obtained data over the entire volume of the sample.

In ref. [18], an extensive comparison was made between the chemical and structural transformations that take place in the mineral composition of cortical and medullary bone during demineralization. The study utilized two-dimensional X-ray diffraction to examine the crystallinity and alignment of apatite crystals. According to the authors, medullary bone mineral, characterized by a disorganized structure and lower crystallinity, undergoes faster dissolution compared to cortical bone mineral. However, the specific changes in the microstructural properties of apatite resulting from demineralization were not quantitatively measured in the study. Furthermore, the authors emphasize that differences in crystallinity alone cannot account for the significant disparity in mineral solubility between these two bone types. They highlight the significant influence of organic matter in the dissolution of bone mineral.

Some publications indicate the formation of other (not apatite) Ca–P phases (crystallographic forms of calcium phosphate) during bone demineralization [14,15]. This is a debatable statement requiring verification, because apatite is the most stable poorly soluble crystalline phase (at pH above 5 it is much less soluble than other calcium orthophosphates [19]); the formation of other phases during the dissolution of apatite depends on the pH of the solution and is unlikely under physiological conditions. In previous works [20–22] we studied the evolution of the crystal microstructure of cortical bone apatite during demineralization, but the parameters determined in these works (crystallite size and lattice microstrain) were not coordinated with the area of active contact of the mineral with the acid agent. In the present work, taking into account SEM-EDX data on the interface or contact zone, we focused on XRD analysis of bone mineral changes in this particular zone. In this work a controlled decrease in the effective depth of the collection of XRD information for the study of partially demineralized cortical bone with a heterogeneous near-surface structure was applied. In addition to this, we considered the possibility to estimate the depth of the reaction front, dividing the demineralized and non-demineralized portions of the bone, by XRD methods.

2. Materials and methods

2.1. Bone samples preparation and demineralization procedure

Bone samples were made from the thighbone of a fully grown cow. The bones were acquired from a nearby butcher shop right after the cow was killed. A section of the middle part of the bone (diaphysis), measuring approximately 4 cm in length and 5 cm in diameter, was immersed in distilled water and heated. Afterwards, it was physically scrubbed to remove any impurities and left to dry in the open air. We chose a large bone in order to have a sufficient amount of homogeneous material. The planar oriented fragments from the middle section of the diaphysis wall were cut out with a laboratory electric saw, their surfaces to be perpendicular to the longer bone

axis. Sizes of the specimens were about 10 × 7 × 3 mm for SEM and 15 × 10 × 3 mm for XRD examinations. Observable surfaces of the specimens were smoothed using sandpaper under the constant water irrigation.

Removal of the mineral from bone can be accomplished using a variety of chemical agents that chelate (ethylenediamine tetraacetic acid, EDTA) or solubilize (hydrochloric acid, HCl) the mineral phase. In our previous work [21], we used HCl and EDTA as demineralizing agents and found that demineralization in EDTA is noticeably slower than in HCl. This is the main difference that can be revealed using XRD. Since the overwhelming majority of works known to us use only HCl [e.g. 13,15,16,18], we decided to use this agent in this work. This allows to compare our results with those of other authors. Actually, the decalcifying agent was 0.1 mol L^{-1} HCl water solution. The stepwise demineralization was made at room temperature in 2 L of the solution stirred constantly. The solution pH was about constant during the demineralization process. After treatment the specimens were washed in distilled water and dried in air. Washing of the samples was carried out simply to remove residual HCl from the surface and pores/cavities/pockets to stop active demineralization processes and fix the state of the samples, but not to eliminate chlorine that has penetrated into the bone matrix.

The surfaces of the samples prepared for XRD analysis were always larger than the cross section of the X-ray probe.

Some details of the samples treatment are described in our previous articles [20,21] and in the next sections of this work.

2.2. SEM and EDX observation

After the demineralization (immersion) procedure, the bone fragment was cut in the plane perpendicular to surface and the cross section (Fig. 1) of the cortical bone was studied by SEM-EDX. The cut surface was not treated/perfected mechanically or chemically to avoid contamination. Before analysis, the bone fragment was mounted on a stub with conductive glue and gold coated. It was analyzed using a scanning electron microscope (Nova NanoSEM 450) coupled with an energy-dispersive X-ray spectrometer with X-Max Silicon Drift Detector (SDD) and ultra-thin window (Oxford Instruments, United Kingdom). The spectral resolution of EDX spectrometer is 124 eV; the active area of SDD is 20 mm^2. Measurements were made with a beam accelerating voltage of 15 kV, emission current of 121 μA, pressure in sample chamber of $1.15{\cdot}10^{-3}$ Pa and a working distance of 8 mm.

2.3. XRD

X-ray measurements are presented in Section 3.2 were carried out with Ni-filtered CuKα radiation by Siemens diffractometer D 5000 with a conventional Bragg-Brentano geometry. Current and voltage on the X-ray tube were 30 mA and 40 kV, respectively. A micrometer screw was used to carefully mount the specimens so that their flat surfaces could meet tangentially with a focusing circle of the diffractometer. The mounting accuracy was about 10 μm. The specimens were scanned in continuous mode over the range of 2θ angles (θ being the Bragg angle) from 10° to 60° to obtain a general diffraction pattern. Scanning was performed with 0.05° step and 1°/min scan speed. All procedures of the data processing were carried out with commercial X-ray diffraction software (DIFFRACplus, Bruker AXS, Karlsruhe, Germany).

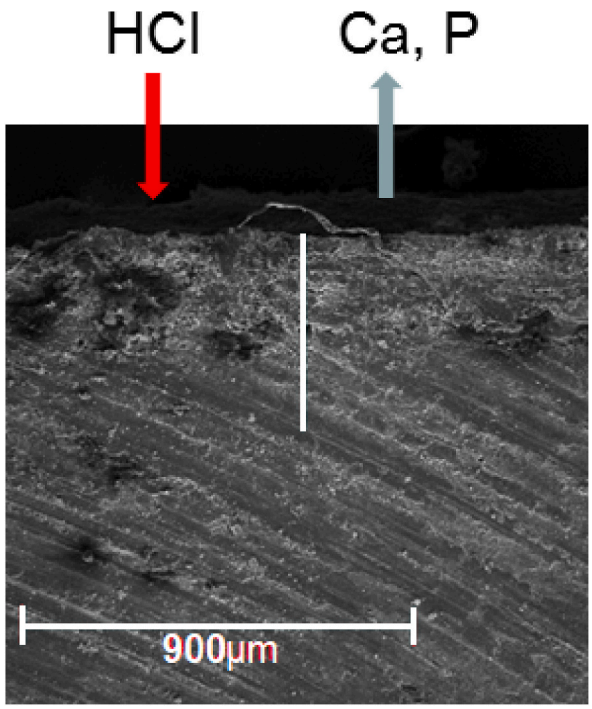

Fig. 1. SEM image of cross-sections of cortical bone after 4 h exposure.

The XRD data represented in Section 3.3 were gained by using the X-ray diffractometer DRON-4-07 (*Burevestnik*, www.bourevestnik.ru) connected to a computer-aided system for experiment control and data processing. The CoKα radiation was used with the conventional Bragg-Brentano focusing method while CuKα radiation was used with the asymmetric geometry for recording diffraction patterns with a sufficiently small (glancing) angle of incidence (α) of the primary beam. The current and the voltage of the X-ray tube were 20 mA and 40 kV, respectively. Scanning was performed in a continuous registration mode with 0.05° step and 1°/min scan speed in 2θ range of 10°–60°. All experimental data were processed in the DifWin-1 program package (Etalon-TC, www.specord.ru). Phase identification was performed using JCPDS (Joint Committee on Powder Diffraction Standards) card catalog. The microstructure of bone apatite was evaluated by separation of contributions from crystallite sizes (L) and lattice microstrains (ε) to a diffraction peak broadening using a pair of diffraction lines [23,24]. Actually the analysis was performed with the "threefold convolution" method using second and fourth order reflections of type (*00l*) Bragg plane, namely (002) and (004), that correspond to the planes oriented along the same crystallographic direction [23]. In this method we used the Voigt function which is a convolution of the Cauchy and the Gaussian functions, namely Voigt integral breadth. The calculations took into account instrumental factors (equipment parameters).

The certain details of the X-ray diffraction experiments are described in the next sections of this work.

3. Results and discussion

3.1. SEM-EDX characterization of partially demineralized cortical bone

The near-surface area of a partially demineralized fragment of cortical bone is (as can be seen from Figs. 1 and 2) an altered organic matrix with a rather low concentration of bone mineral elements. The depth of this layer can reach 150–200 μm from the sample surface already after 4 h of demineralization (immersion) in 0.1 mol L^{-1} HCl solution. Separate synchronous bursts of Ca and P concentrations in the demineralized layer, in our opinion, are mainly the result of contamination of the cut surface with microscopic particles of the mineral during mechanical cutting of the sample, and to a lesser extent can be attributed to apatite residues in the organic matrix that were not washed out by the solvent. It should be noted that Fig. 2 shows the raw EDX line scan data, which semi-quantitatively reflect changes in element concentrations along the scan line. Calculation of element concentrations using standards and the ZAF correction method was not carried out.

SEM-EDX observations were repeated several times for both the original and demineralized samples to ensure the homogeneity of the materials. In all cases, we observed a qualitatively identical picture.

In order to highlight the trends of the concentration changes and achieve greater illustrativeness of the EDX-scan data, we

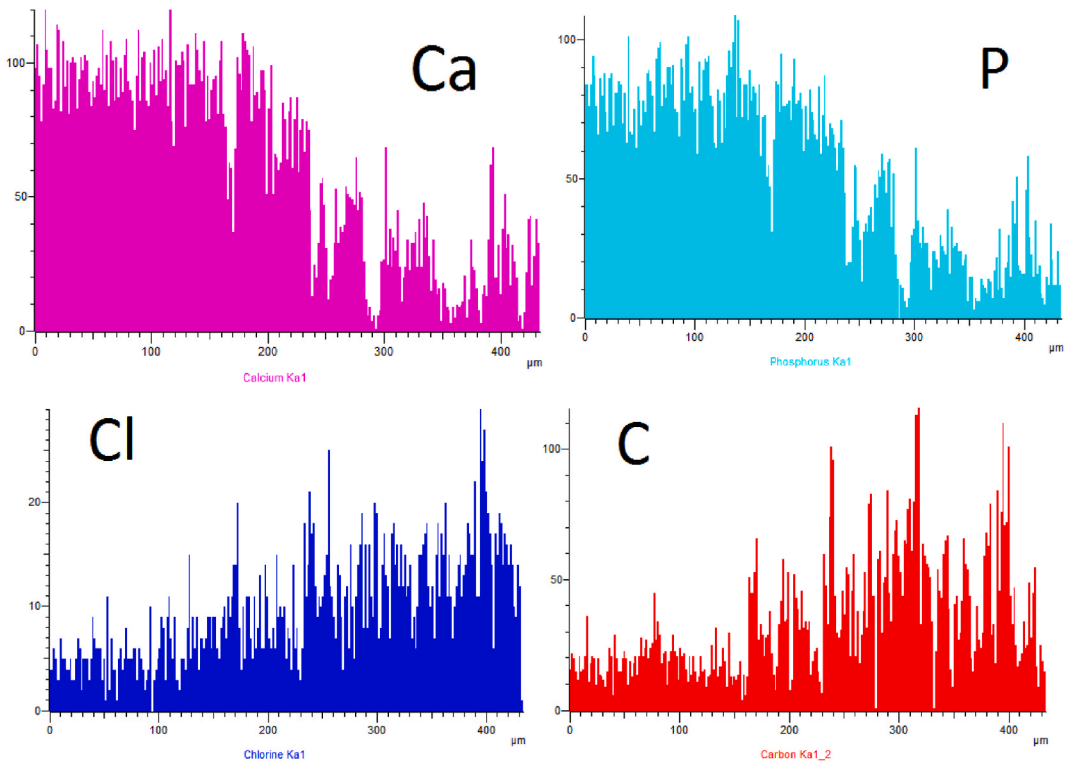

Fig. 2. Raw results of EDX line scan analysis (the main elements: Ca, P, Cl, C) of a cortical bone section along the vertical line shown in Fig. 1 (scan line length 435 μm).

performed the procedure for smoothing the concentration profiles using the OriginPro 9.2 program. This made it possible to distinguish, as in Ref. [15], three different zones (Fig. 3): demineralized matrix (DM), middle interface zone (IZ), and mineralized matrix (MM) and evaluate changes in their size during stepwise demineralization.

Most of the smoothed profiles show quite clearly that the middle contact (interface) zone (IZ) can be conventionally divided into IZ1 layer and IZ2 layer (Fig. 3). The cross section of the IZ2 layer is characterized by a linear decrease in the concentration of Ca and P in the direction from MM to DM and an increase in the concentration of chlorine penetrating from the decalcifying solution. In the IZ1 layer, with the same behavior of chlorine, the concentrations of Ca and P remain almost at the level of the MM zone with a barely noticeable tendency to decrease in the direction of IZ2. Obviously, it is in IZ1 that the initial stage of the interaction of the decalcifying solution with the bone mineral occurs, which can cause certain slight alteration in bioapatite crystals, but does not lead to significant changes in the Ca and P concentrations due to the inertia of the processes of dissolution and mass transfer. At the same time, the Ca and P concentration gradient in the IZ2 layer points to the usual diffuse mechanism for the removal of dissolved mineral components to the sample surface and to the solution surrounding it. There is a noticeable trend towards more accelerated dissolution and transport of calcium compared to phosphorus, which is consistent with the data of other studies [22,25,26]. In general, the data obtained indicate that it is the dissolution of crystals, and not the diffusion of mineral residues from the volume of the bone to its surface, that is the factor limiting demineralization.

Fig. 3 shows that after 4 h of demineralization in a 0.1 mol L^{-1} HCl solution, the thickness of the IZ2 layer is approximately 135 μm, the total thickness of the IZ layer, where a linear decrease in the chlorine concentration is observed in the direction from DM to MM, is ~240 μm, and the thickness of the demineralized DM layer is ~145 μm. These quantitative indicators are in agreement with the results of [15], where DM ~ 130 μm after 2 h exposure in 0.5 M HCl and ~400 μm after 4 h in 2 M HCl. According to our data, as well as works [15], with an increase in the immersion time, not only an increase in the zone of completed demineralization DM is observed, but also an expansion of the interface layer IZ, i.e., "blurring" of the interaction zone. It should be noted that the above sizes of the selected layers can be considered only approximately, since in the samples analyzed by us they are characterized by a certain scatter of values. At the same time, we consider it appropriate to present our data on the change in the thickness of the IZ2 layer during stepwise demineralization of one of the typical samples of cortical bone in 0.1 mol L^{-1} HCl solution (Table 1).

3.2. Features and limitations of X-ray diffraction analysis of partially demineralized cortical bone

X-ray diffraction methods have been used previously in several studies to assess the effect of acid concentration and immersion duration on cortical bone demineralization [16,17,20]. Their authors noted that the decrease in the intensity of the diffraction peaks of apatite and the broadening of their profile during demineralization are caused by the degradation of the crystal lattice and the removal of the mineral from the bone matrix. In addition, in our work [20], it was shown that a decalcified layer on the bone surface causes a shift in the position of diffraction lines and a decrease in their intensity due to absorption. The formation of the decalcified layer on the bone surface due to the advance of the reaction front into the tissue is a complicating feature of XRD analysis of partially demineralized planar bone specimens. In this work, we tried to use the effects of shifting diffraction lines and reducing their intensity caused by the decalcified layer to estimate its thickness.

To do this, five cortical bone samples (close fragments of one shaft of a bovine femur, ca. 15 × 10 × 3 mm) were subjected to a stepwise demineralization procedure in 0.1 mol L^{-1} HCl solution, with X-ray diffraction patterns being recorded after each stage. All peaks of the diffraction patterns of the untreated specimens correspond to the hydroxyapatite lattice ($Ca_{10}(PO_4)_6(OH)_2$, JCPDS 9-432). From the processing of the obtained five series of X-ray diffraction patterns (Fig. 4 shows one of the series), a linear relationship was found between the duration of immersion and the shift in the position of the diffraction lines (Fig. 5).

It should be noted that the analyzed surfaces were perpendicular to the longitudinal axis of the bone, and the demineralization front moved inward from this surface (as in Fig. 1). This made it possible, using the natural texture of biological apatite, to obtain intense

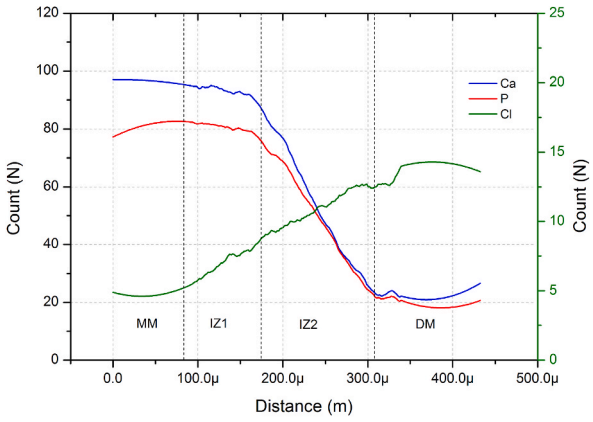

Fig. 3. Typical example of smoothed concentration profiles for Ca, P and Cl obtained from EDX linescan of a cortical bone section (treatment time 4 h; vertical left axis scale corresponds to Ca and P, right axis scale corresponds to Cl).

Table 1
Thickness of IZ2 layer in acid-treated cortical bone evaluated by SEM coupled with EDX.

Duration of demineralization, hours	1	2	4	5
IZ2 layer thickness, μm	35	110	135	175

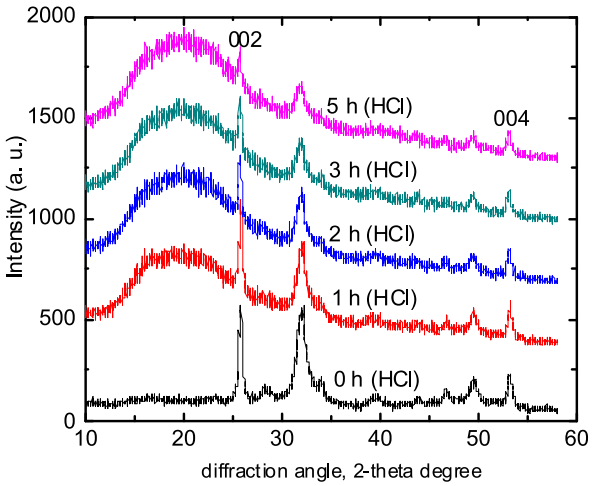

Fig. 4. X-ray diffraction patterns of partially demineralized (initial and stepwise-demineralized) cortical bone after different immersion times in 0.1 mol L^{-1} HCl solution.

reflections from the (002) and (004) basal planes, which were used in the analysis.

The effect of the angular shift of diffraction lines ($\Delta 2\theta$) of a partially demineralized cortical bone sample is similar to the mechanical displacement of the sample in the radial direction from the normal position on the focusing circle (Fig. 6). The surface layer of the bone after the removal of the mineral component is an organic matrix (DM in Fig. 3) devoid of apatite crystals, and the crystals involved in the formation of the diffraction pattern are situated deeper under the surface. Here we simplify the object to a two-layer model without a transitional layer. In this case, the distance between the surface of the sample and the depth of occurrence of "reflecting" crystals (τ) can be estimated by formula (1) [27]:

$$\Delta 2\theta = -\frac{2\tau \cdot \cos\theta}{R}, \quad (1)$$

where R is the radius of the goniometer circle (R = 200,5 mm for Siemens D 5000) and θ one half of the Bragg angle.

The additional measurements were carried out, in which the influence of the specimen displacement on the shape and angular position of the (200) diffraction line of powdered NaCl was studied. The specimen was displaced down in the radial direction from the focusing circle center (FC in Fig. 6) with a mounting micrometer screw. The displacements up to 100 μm led to linear shifts in the

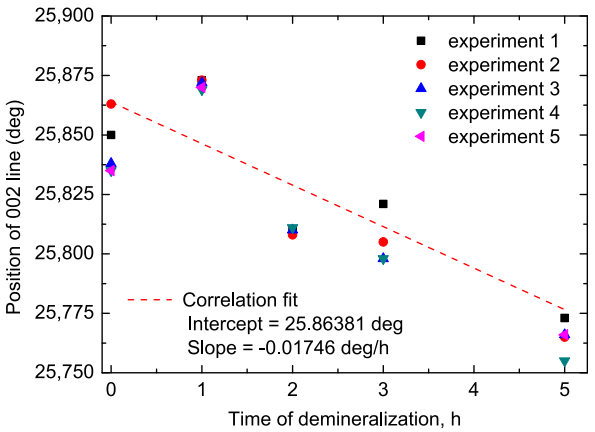

Fig. 5. Change in the position of the diffraction line (002) of bioapatite depending on the duration of demineralization according to the data of five experiments (straight line – linear approximation of experimental points by standard deviation).

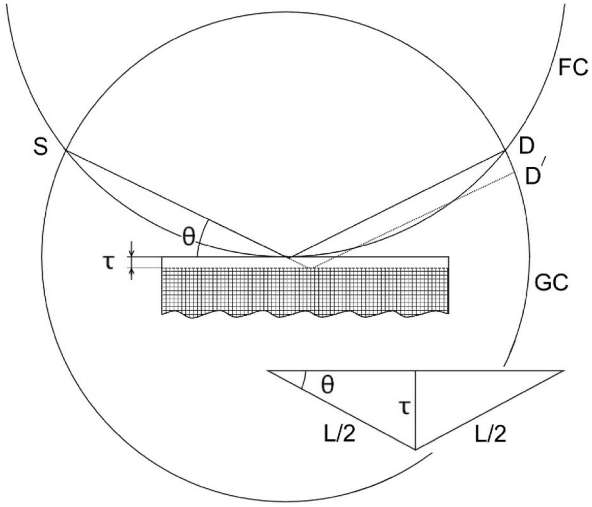

Fig. 6. Scheme of diffraction with symmetric geometry (at θ-2θ focusing) under conditions of formation of a demineralized layer with a thickness of τ, S is the focus of the X-ray tube, GC is the goniometer circle, D is the radiation detector, DD' is displacement of the detector position due to deepening of the crystals from the surface to the depth τ, L is the length of the radiation path in the demineralized layer.

positions of the diffraction line with no apparent effect on the intensity and width at half maximum. This result reinforces our suggestion that the line shift can be used to estimate the depth of the reaction front dividing the demineralized and non-demineralized parts of the bone.

From the angular shifts of the (002) line of bone apatite ($\Delta 2\theta_{002}$) (Fig. 5), the thicknesses of the demineralized layer (τ_{sh}) and the X-ray path lengths in this layer ($L = 2\tau/\sin\theta$) were obtained for the corresponding diffraction angle depending on the duration of the demineralization process (Table 2). The data obtained are consistent with our own and available from literature SEM-EDX evaluations [15]. Although these data do not allow us to detail the complex structure of the demineralized bone subsurface, including transitional layers, they can serve as a semi-quantitative indicator of advancing reaction front. This method of estimation can be useful in cases where the sample must not be destroyed, or when information on the average thickness of the demineralized layer is required instead of just the local information obtained by a microscope.

The formation of a demineralized layer dividing the surface of a bone sample and crystals causes not only a shift of diffraction lines, but also a decrease in their intensity due to partial absorption of radiation in this "translucent" layer during the passage of path L (Fig. 6). This effect is superimposed on a decrease in the intensity of lines due to acid destruction of crystals. The removal of the organic component from the bone seems to be a reasonable way to get rid of the formation of the decalcified layer on the bone surface, which leads to a shift and a decrease in the intensity of the diffraction lines. It is reasonable to assume that the rate of dissolution of bone apatite crystals depends little on the organic component of the tissue. This is supported by the SEM-EDX data, which indicate that it is the dissolution of crystals, and not the diffusion of acid into the volume of the bone and mineral elements to its surface, that limit the rate of demineralization. To clarify the situation, we took XRD examination of stepwise demineralized (0.1 mol L^{-1} HCl solution) cortical bone with the organic component previously thermally decomposed (annealing at 450 °C for 1 h). Such moderate annealing destroys the organic component of the tissue, leaving the bone mineral unchanged [28]. The corresponding series of X-ray diffraction patterns is shown in Fig. 7. For this series of samples, in contrast to samples of native bone, no halo formation (at angles of $2\theta \approx 20°$) and no shift of diffraction lines during demineralization were observed; the integral intensity of the lines somewhat decreased with the time of immersion, but to a much lesser extent than in the case of the unannealed/original bone (Fig. 8). If the decrease in the intensity of the lines of a native bone from the two above-mentioned causes has an additive character, then by simple arithmetic subtraction, it is possible to separate the component of the decrease in intensity due to absorption in the demineralized layer.

Thus, according to the data on the relative decrease in intensity (Fig. 8), corrected for the decrease in intensity for a pre-annealed sample, due only to the degradation of crystals, one can try to estimate the thickness of the absorbing demineralized layer ($\tau = ½\cdot L\bullet\sin\theta$) using the known formula (2) [29]:

$$I_\tau = I_0 e^{-(\mu/\rho)\rho L}, \tag{2}$$

Table 2
The effective thickness of the demineralized layer and the total X-ray path in it for the (002) reflex depending on the immersion time of the sample, calculated from the angular shift of the diffraction line.

Duration of demineralization, hours	1	2	3	5
τ_{sh} layer thickness, μm	31.5	62.7	94.0	156.7
$L = 2\tau/\sin\theta$, μm	282.2	561.7	842.1	1403.8

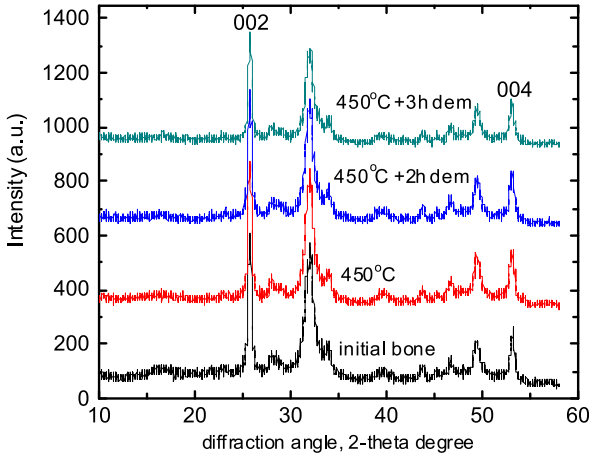

Fig. 7. X-ray diffraction patterns of the original and pre-annealed cortical bone after different exposure times in 0.1 mol L^{-1} HCl solution (2 and 3 h).

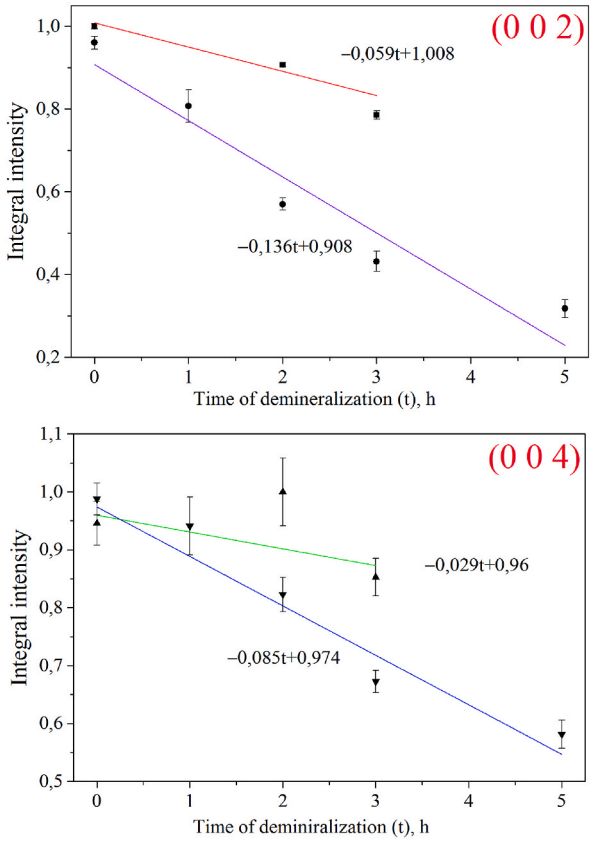

Fig. 8. Change in the relative (normalized) intensity of the diffraction lines (002) and (004) on the time of demineralization (t) for samples of native and pre-annealed cortical bone (straight lines – linear approximation of experimental points by standard deviation, lower lines – native bone, top lines – pre-annealed bone). The values presented were obtained by processing five series of X-ray diffraction patterns for both types of specimens; error bars show that the total error in most cases did not exceed 10%.

where I_0 is the normalized intensity of the line (00l) of the original ($t = 0$ h) sample, I_τ is the normalized intensity of the line (00l) of the sample with a demineralized layer on the surface, reduced by the effect of weakening the "reflection" due to the destructive change of crystals, μ/ρ is the mass absorption coefficient of X-ray in the demineralized tissue (for CuKα), ρ is the density of the absorbing substance. Taking into account that the demineralized layer consists mainly of collagen, water, and negligible mineral residues, and

using reference data from the literature [30,31], the parameters necessary for calculation were chosen as follows: $\rho = 1.24$ g/cm^3; $\mu/\rho = 3.49$ cm^2/g. The calculation results are presented in Table 3.

From a comparison of Table 3, Tables 2 and it can be seen that τ_{int} have slightly lower values than τ_{sh}, especially with a short demineralization time. This may be due to several reasons: an overestimated value of μ/ρ, insufficient validity of the assumptions made, a statistical discrepancy between the two arrays of experimental data, etc. In both cases we ignore the interface zone and neglect X-ray adsorption in the remaining mineral. However, in general, the τ_{int} and τ_{sh} are in good agreement, which indicates a correct interpretation of the physical reasons for the decrease in intensity and shifts of diffraction lines.

A close examination of the graphs presented in Fig. 8 shows that during demineralization, the decrease in the intensity of the (002) line occurs faster than the (004) line for both native and annealed bone. This is explained by the difference in the depth of the effectively reflecting layer for different diffraction angles, in this case $2\theta_{002}$ and $2\theta_{004}$. In the case of the line (002), the penetration depth is less than for the line (004) and the information obtained corresponds to the layers of apatite more influenced by acid attack. With an increase in the diffraction angle, the penetration depth of the radiation increases and the obtained X-ray diffraction information corresponds to deeper layers of apatite, which are changed to a lesser extent. The issue of the depth of the material's layer involved in the formation of the diffraction pattern in the case of partially demineralized cortical bone will be considered in more detail in the next section of this work. Now, it is necessary to note two important conclusions following from the analysis of the data in Fig. 8: (1) destructive changes in apatite due to acid attack are surface-gradient, that is, near-surface crystals are more destructured than deeper ones; (2) joint analysis of the physical broadening of the (002) and (004) lines for the simultaneous determination of the crystallite size and microstrain of the apatite lattice (L_{00l} and ε_{00l}) [23] may be incorrect due to the different depth of the effectively reflecting layer for different diffraction angles and differences in microstructural parameters in different layers (for example, IZ1 and IZ2 in Fig. 3).

This encourages us to study the question of the depth of the material's layer involved in the formation of the diffraction pattern ("effective penetration depth") for such a complex object as a partially demineralized cortical bone. Only if the effective penetration depth for the both lines (002) and (004) approximately corresponds to the depth of the layer with equally modified bone apatite (for example, IZ1 in Fig. 3), the analysis of microstructural changes during demineralization will be correct. At the same time, the use of physical broadening of single lines for estimating the size of bioapatite crystallites according to Scherrer [27] (ignoring the lattice microdeformation factor) is not limited in any way, which can serve as a quantitative indicator of microstructural changes in the bone mineral during demineralization. The results of such estimates are presented in our previous paper [21].

3.3. *Effective radiation penetration depth and structural characteristics of partially demineralized cortical bone*

As can be seen, partially demineralized cortical bone is a complex object for X-ray diffraction studies due to the presence of a superficial demineralized layer (DM) and a transition zone (IZ) with a gradient of concentration and structural characteristics (Fig. 3). Obtaining structural characteristics that reflect changes in the mineral caused by acid attack requires controlling the depth of the material's layer involved in the formation of the diffraction pattern. Particular care is required in the application of methods for determining microstructural parameters (L and ε) from the analysis of a pair of diffraction lines corresponding to different reflection orders. The dependence of the penetration depth of the primary X-ray beam on the diffraction angle 2θ leads to the fact that the probing depth increases with an increase in the indices hkl. A controlled decrease in the probing depth in diffraction studies can be implemented in two ways: a special "glancing-angle" geometry and/or long-wave (soft) primary radiation [29,32].

To estimate the depth of the layer of the material participating in the formation of the diffraction pattern (briefly, "effective penetration depth", h), in the symmetric Bragg-Brentano (θ-2θ) geometry, an equation is usually used, which is a consequence of the exponential law of radiation absorption in matter (3) [29]:

$$h = -\ln(I_h / I_0)\frac{\sin\theta}{2(\mu/\rho)\cdot\rho}, \ln(I_h / I_0) = -2\left[(\mu/\rho)_{mm}\rho_{mm}\cdot\frac{h_{mm}}{\sin\theta} + (\mu/\rho)_{dm}\rho_{dm}\cdot\frac{h_{dm}}{\sin\theta}\right], \quad (3)$$

where μ/ρ is the mass absorption coefficient of X-ray radiation in the material under study, ρ is the density of the material, I_h/I_0 is the relative attenuation of radiation due to absorption in the h layer. When a thin, weakly absorbing layer (demineralized matrix) of thickness h_{dm} is formed on the surface of a more roentgen-dense material (mineralized bone matrix), the probing depth of the mineral matrix h_{mm} will slightly decrease due to absorption in the demineralized matrix. For a simplified two-layer model that neglects the transition region IZ, the dependence of radiation absorption on h_{dm} and h_{mm} can be represented by formula (4):

Table 3
The thickness of the demineralized layer, calculated from the relative changes in the integrated intensity of the lines (002) and (004), depending on the time of immersion of the sample (τ_{int}).

Duration of demineralization, hours	1	2	3	4	5
L_{002}, μm	227.9	457.0	710.5	994.7	1318.8
L_{004}, μm	38.6	178.6	327.7	487.0	657.9
Thickness of layer τ_{002}, μm	25.4	51.0	79.2	110.9	147.0
Thickness of layer τ_{004}, μm	8.6	39.8	73.1	108.6	146.7

$$\ln(I_h / I_0) = -2\left[(\mu/\rho)_{mm}\rho_{mm} \cdot \frac{h_{mm}}{\sin\theta} + (\mu/\rho)_{dm}\rho_{dm} \cdot \frac{h_{dm}}{\sin\theta}\right], \quad (4)$$

where $(\mu/\rho)_{dm}$ and $(\mu/\rho)_{mm}$ are the mass absorption coefficients of the demineralized matrix and normal mineralized bone material, respectively; I_h/I_0 is the relative radiation attenuation due to absorption in $h_{dm} + h_{mm}$. Then, for such a two-layer model, h_{mm} can be calculated using formula (5):

$$h_{mm} = \frac{1}{(\mu/\rho)_{mm} \cdot \rho_{mm}}\left[\ln(I_0 / I_t)\frac{\sin\theta}{2} - (\mu/\rho)_{dm} \cdot \rho_{dm} \cdot h_{dm}\right], \quad (5)$$

Formula (5) makes it possible to estimate the information depth or thickness of the biological apatite layer, which takes part in the formation of the diffraction pattern, for a two-layer sample, the near-surface region of which (thickness h_{dm}) is free of the mineral and does not contribute to the diffraction pattern of apatite, but only absorbs X-rays. For the demineralized layer, as in the previous section (subsection 3.2), we take $(\mu/\rho)_{dm} = 3.49$ cm^2/g (for CuKα), $\rho_{dm} = 1.24$ g/cm^3, while for the mineralized bone matrix, based on literature data [31], we take the following values: $(\mu/\rho)_{mm} = 35.25$ cm^2/g (for CuKα), $\rho_{mm} = 1.85$ g/cm^3. Based on the SEM-EDX data presented above and the estimates made by XRD (Tables 2 and 3), we believe that h_{dm} is approximately 80 μm and 150 μm after demineralization in 0.1 mol L^{-1} HCl solution for 3 h and 5 h, respectively. With these assumptions, using formulas (3) and (4), the penetration depth calculations were performed, the results of which are presented in Fig. 9. These data demonstrate a strong dependence of the depth of X-ray probing on the diffraction angle 2θ and the I_h/I_0 ratio, which is determined to a large extent by the detection system of the instrument. The representation as a three-dimensional dependence is due to some uncertainty of the ratio I_h/I_0, which forces the researchers in practice to choose a certain conditional value from general considerations or to determine this ratio experimentally from the analysis of two-layer samples with a known thickness and material of the outer layer (coating). From the estimates we made using model samples [32], it follows that $I_h/I_0 = 0.2$ can be a reasonable alternative. At this, as can be seen from the calculations (Fig. 9), the change of CuKα radiation to CoKα for the original (not demineralized) bone reduces the penetration depth quite significantly: from 27–62 μm to 17.5–40.5 μm. The values $(\mu/\rho)_{mm}$ and $(\mu/\rho)_{dm}$ for CoKα were recalculated taking into account the additive nature of the X-ray attenuation coefficient in the material [30,31,33]. The formation of a weakly absorbing layer of demineralized matrix on the sample surface slightly reduces the thickness of the bioapatite layer involved in the formation of the diffraction pattern (h_{mm}). Diffraction lines (002) and (004) correspond to slightly different values of the penetration depth, but when using CoKα radiation, the calculated values of h_{mm} do not go beyond the transition zone (IZ, Fig. 3). It should be noted that in the case of a real partially demineralized cortical bone, the penetration depth will be slightly larger than calculated here for the simplified two-layer model (DM + MM) due to slightly lower values of $(\mu/\rho)_{iz}$ and ρ_{iz} of the IZ zone relative to $(\mu/\rho)_{mm}$ and ρ_{mm}. However, from a comparison of the results of the performed assessments with the SEM-EDX data, it is clear that the structural information obtained from XRD relates mainly to the IZ zone of active interaction of the acid agent with the bone mineral.

Our estimates show that the use of a "softer" radiation (for example, CoKα instead of CuKα) significantly reduces the probing depth, that can serve as a means of increasing the correctness of determining microstructural parameters (L and ε) in the IZ transition zone of partially demineralized bone. In any case, the structural information obtained from X-ray diffraction studies of such surface-gradient objects as partially demineralized cortical bone should be analyzed together with estimation of the effective penetration depth.

Taking into account the circumstances considered here, we carried out XRD studies of changes in microstructural parameters of

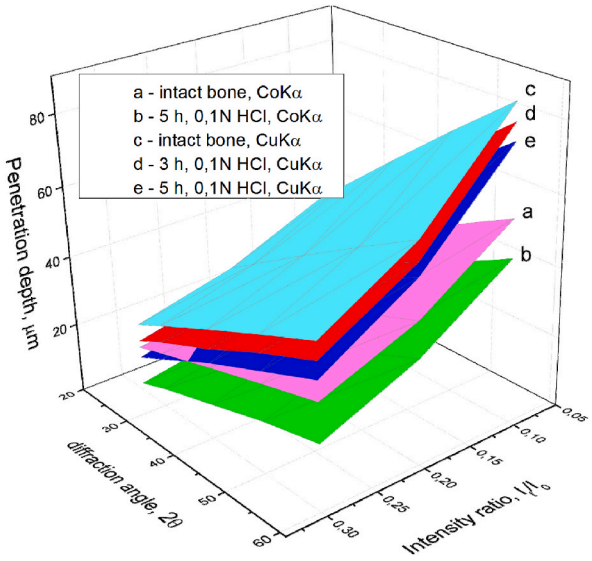

Fig. 9. Dependence of the penetration depth on the diffraction angle 2θ and the ratio I_h/I_0 for the intact and partially demineralized cortical bone, calculated by formulas (3) and (4) for different probing radiation (*CoKα*, *CuKα*).

partially demineralized cortical bone. To reduce the probing depth, we used CoKα radiation, and stepwise demineralization was carried out in a relatively weak acid solution (0.02 mol L^{-1} HCl versus 0.1 mol L^{-1} HCl in previous experiments). A decrease in the acid concentration, according to our SEM-EDX observations, significantly slowed down the reaction front advance rate and expanded the IZ transition zone. Quantification of these changes is difficult due to the blurring of the boundaries of the IZ and DM zones, but these qualitative patterns are quite obvious. This ensured that we obtained X-ray diffraction data from the IZ transition region with approximately equivalent bioapatite alterations due to acid attack.

Fig. 10 shows the revealed evolution of both parameters of the microstructure, though it is important to note that the obtained numerical values are not absolute, but only "effective values" and cannot be used for a full-fledged quantitative analysis. We believe that the error of the method makes it possible to reveal a general trend in the evolution of the parameters.

Our result shows that acid demineralization of the cortical bone occurs with a nonmonotonic decrease in the average size of crystallites (L) and lattice microstrains of apatite (ε). At the first stage of demineralization, the dissolution of smaller and more defective crystals occurs, as a result of which the average L increases, and ε decreases. Subsequently, larger crystals also dissolve, but those with greater defectiveness are preferable. These findings are in good agreement with the results of other works [18,20,21], in which a more detailed discussion is presented. Although in Ref. [18] these conclusions were made on the basis of a comparison of acid-induced demineralization of two radically different samples: cortical and medullary bone.

To study the phase composition of the altered mineral of the IZ transition zone, we applied of asymmetric or "glancing-angle" geometry with a sufficiently small (glancing) angle of incidence of the primary x-ray beam (α), which makes it possible to significantly reduce the penetration depth h. In that case, h can be estimated using the following formula (6) [29]:

$$h = \frac{\ln(I_0/I_h)}{(\mu/\rho)\cdot\rho}\cdot\frac{\sin\alpha\cdot\sin(2\theta-\alpha)}{\sin\alpha+\sin(2\theta-\alpha)}. \quad (6)$$

From the performed calculations, it follows that for an intact (non-demineralized) cortical bone at CuKα radiation, h will be only 7.2–7.9 μm, 9.8–11.4 μm and 11.6–14.6 μm at angles α equal to 4°, 6° and 8°, respectively. The formation during demineralization of the DM layer and the IZ transition zone slightly increases the probing depth of the affected mineral, while maintaining a confident possibility of shallow analysis. Fig. 11 shows X-ray diffraction patterns of the original cortical bone and the same bone demineralized in 0.02 mol L^{-1} HCl solution for 96 h, taken with asymmetric geometry at angles α equal to 4°, 6°, 8° and 10°. As can be seen, the phase composition of the near-surface layers of the original and partially demineralized cortical bone is identical; no crystalline phases other than poorly crystalline apatite (JCPDS 9 432) are found in the transition zone IZ. The decrease in the intensity of the lines (002) and (004) with decreasing angle α is caused by the deviation from the top of the texture maximum at asymmetric geometry. For a demineralized sample, the line intensities decrease with decreasing α even more strongly, because in this case, the probing depth also decreases. This confirms the gradient nature of the mineral's structural alterations in the IZ transition zone.

It necessary to note that the asymmetric or "glancing-angle" method is widely used for phase analysis of thin films, multilayers materials and near-surface regions of surface-modified materials [29,34,35], and is limitedly suitable for the analysis of diffraction line broadening due to aberration of focusing conditions in the case of using conventional (not special) XRD instruments. In our work, the depth-controlled XRD analysis was applied for the first time to such a complex (surface-gradient) object as partially demineralized cortical bone.

4. Conclusions

In this work, the SEM-EDX and XRD methods were used to study the process of bone mineral deterioration under the influence of a chemical agent, which, in the first approximation, can simulate the consequences of such biological phenomena as osteoporosis or bone loss in weightlessness. The conclusions drawn on the basis of the results of the study of the stepwise demineralization of the cortical bone can be formulated as follows:

(1) during acid demineralization of the cortical bone, the "reaction front" separating the demineralized matrix from the mineralized tissue progressively moves away from the interaction surface, and its movement speed is close to linear;
(2) between DM and MM, a transition interface zone IZ is formed, possessing a concentration and structural gradient, the width of which increases with the duration of the interaction;
(3) the physicochemical process that limits demineralization is the dissolution of bioapatite crystals, and not the diffusion of dissolved mineral ions from the volume to the surface of the bone;
(4) the physical broadening of the diffraction lines of bioapatite can serve as a semi-quantitative indicator of microstructural changes in the bone mineral during demineralization, provided that the informative depth of the diffraction pattern corresponds to the dimension of the transition zone between DM and MM;
(5) application of asymmetric or "glancing-angle" XRD geometry with a sufficiently small angle of the incidence beam shown that the phase composition of the near-surface layers of the intact and partially demineralized cortical bone is identical; no crystalline phases other than poorly crystalline bioapatite are found in the transition zone IZ.

Author contribution statement

Sergei Danilchenko: Conceived and designed the experiments; Analyzed and interpreted the data; Wrote the paper.

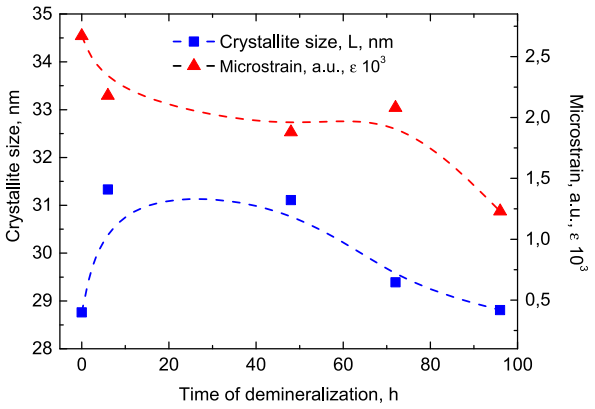

Fig. 10. Dependence of microstructural parameters (L_{00l} and ε_{00l}) of partially demineralized cortical bone on the duration of stay in 0.02 mol L^{-1} HCl solution obtained using CoKα radiation. The points are the average values obtained from the processing of five series of X-ray diffraction patterns; the error was about 10%; the dashed lines are drawn only to indicate general tendency.

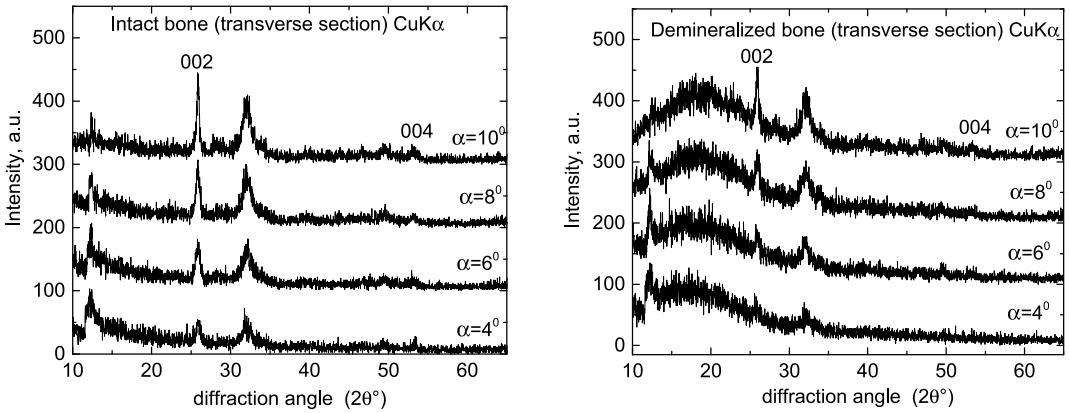

Fig. 11. X-ray diffraction patterns of the intact (right) and partially demineralized cortical bone (96 h in 0.02 mol L^{-1} HCl solution, left) taken using CuKα radiation with asymmetric geometry at angles α equal to 4°, 6°, 8° and 10°.

Aleksei Kalinkevich: Analyzed and interpreted the data; Wrote the paper.
Mykhailo Zhovner, He Li, Aleksandr Kochenko: Performed the experiments.
Petro Danylchenko: Analyzed and interpreted the data.
Jufang Wang: Conceived and designed the experiments; Contributed reagents, materials, analysis tools or data.

Data availability statement

The raw/processed data required to reproduce these findings cannot be shared at this time due to technical or time limitations.

Declaration of competing interest

The authors declare that they have no known competing financial interests or personal relationships that could have appeared to influence the work reported in this paper

Acknowledgements

This work was partially supported by grants from the National Natural Science Foundation of China (No. 31870851) and the International Science & Technology Cooperation Program of China (No. 2015DFR30940).

References

[1] J. Rubin, E.M. Greenfield, in: F. Bronner, M.C. Farach-Carson, J. Rubin (Eds.), Osteoclast: Origin and Differentiation, Bone Resorption, Springer, London, 2005, pp. 1–23.

[2] S.L. Teitelbaum, Bone resorption by osteoclasts, Science 289 (2000) 1504–1508.
[3] G.A. Rodan, T.J. Martin, Therapeutic approaches to bone diseases, Science 289 (2000) 1508–1514.
[4] A.L. Boskey, Variations in bone mineral properties with age and disease, J. Musculoskelet. Neuronal Interact. 2 (2002) 532–534.
[5] H. Fonseca, D. Moreira-Gonçalves, H.-J.A. Coriolano, J.A. Duarte, Bone quality: the determinants of bone strength and fragility, Sports Med. 44 (2014) 37–53.
[6] D. Uebelhart, J. Bernard, D.J. Hartmann, L. Moro, M. Roth, B. Uebelhart, L. Vico, Modifications of bone and connective tissue after orthostatic bedrest, Osteoporosis Int. 11 (2000) 59–67.
[7] M. Inoue, H. Tanaka, T. Moriwake, M. Oka, C. Sekiguchi, Y. Seino, Altered biochemical markers of bone turnover in humans during 120 days of bed rest, Bone 26 (2000) 281–286.
[8] E.R. Morey-Holton, R.K. Globus, Hindlimb unloading rodent model: technical aspects, J. Appl. Physiol. 92 (2002) 1367–1377.
[9] J. He, X. Feng, J. Wang, W. Shi, H. Li, S. Danilchenko, A. Kalinkevich, M. Zhovner, Icariin prevents bone loss by inhibiting bone resorption and stabilizing bone biological apatite in a hindlimb suspension rodent model, Acta Pharmacol. Sin. 39 (2018) 1760–1767.
[10] A. Akbay, G. Bozkurt, O. Ilgaz, S. Palaoglu, N. Akalan, E.C.A. Benzel, Demineralized calf vertebra model as an alternative to classic osteoporotic vertebra models for pedicle screw pullout studies, Eur. Spine J. 17 (2008) 468–473.
[11] C.Y. Lee, S.H. Chan, H.Y. Lai, S.T. Lee, A method to develop an in vitro osteoporosis model of porcine vertebrae: histological and biomechanical study: laboratory investigation, J. Neurosurg. Spine 14 (2011) 789–798.
[12] J.W.A. Fletcher, S. Williams, M.R. Whitehouse, H.S. Gill, E. Preatoni, Juvenile bovine bone is an appropriate surrogate for normal and reduced density human bone in biomechanical testing: a validation study, Sci. Rep. 8 (2018) 1–9.
[13] K.U. Lewandrowski, W.W. Tomford, N.A. Michaud, K.T. Schomacker, T.F. Deutsch, An electron microscopic study on the process of acid demineralization of cortical bone, Calcif. Tissue Int. 61 (1997) 294–297.
[14] D.A. Horneman, M. Ottens, M. Hoorneman, L.A. van der Wielen, M. Tesson, Reaction and diffusion during demineralization of animal bone, AIChE J. 50 (2004) 2682–2690.
[15] V. Sabolová, A. Brinek, V. Sládek, The effect of hydrochloric acid on microstructure of porcine (Sus scrofa domesticus) cortical bone tissue, Forensic Sci. Int. 291 (2018) 260–271.
[16] M. Figueiredo, S. Cunha, G. Martins, J. Freitas, F. Judas, H. Figueiredo, Influence of hydrochloric acid concentration on the demineralization of cortical bone, Chem. Eng. Res. Des. 89 (2011) 116–124.
[17] G.T. El-Bassyouni, O.W. Guirguis, W.I. Abdel-Fattah, Morphological and macrostructural studies of dog cranial bone demineralized with different acids, Curr. Appl. Phys. 13 (2013) 864–874.
[18] N. Dominguez-Gasca, C. Benavides-Reyes, E. Sánchez-Rodríguez, A.B. Rodríguez-Navarro, Changes in avian cortical and medullary bone mineral composition and organization during acid-induced demineralization, Eur. J. Mineral 31 (2019) 209–216.
[19] J.C. Elliott, Structure and chemistry of the apatite and other calcium orthophosphates, in: Studies in Inorganic Chemistry, vol. 18, Elsevier, 1994.
[20] S.N. Danilchenko, C. Moseke, L.F. Sukhodub, B. Sulkio-Cleff, X-ray diffraction studies of bone apatite under acid demineralization, Cryst. Res. Technol. 39 (2004) 71–77.
[21] S. Danilchenko, A. Kalinkevich, M. Zhovner, V. Kuznetsov, H. Li, J. Wang, Anisotropic aspects of solubility behavior in the demineralization of cortical bone revealed by XRD analysis, J. Biol. Phys. 45 (2019) 77–88.
[22] M. Zhovner, A.N. Kalinkevich, S.N. Danilchenko, V.N. Kuznetsov, J. Wang, H. Li, J. He, X. Feng, A mechanical device to evaluate the effects of dynamic loading in weak-acid medium on the bioapatite of devitalized cortical bone, Exp. Tech. 44 (2020) 591–596.
[23] S.N. Danilchenko, O.G. Kukharenko, C. Moseke, I.Y. Protsenko, L.F. Sukhodub, B. Sulkio-Cleff, Determination of the bone mineral crystallite size and lattice strain from diffraction line broadening, Cryst. Res. Technol. 37 (2002) 1234–1240.
[24] C. Meneghini, M.C. Dalconi, S. Nuzzo, S. Mobilio, R.H. Wenk, Rietveld refinement on X-ray diffraction patterns of bioapatite in human fetal bones, Biophys. J. 84 (2003) 2021–2029.
[25] H. Pan, J. Tao, X. Yu, L. Fu, J. Zhang, X. Zeng, G. Xu, R. Tang, Anisotropic demineralization and oriented assembly of hydroxyapatite crystals in enamel: smart structures of biominerals, J. Phys. Chem. B 112 (2008) 7162–7165.
[26] W.J. Tseng, C.C. Lin, P.W. Shen, P. Shen, Directional/acidic dissolution kinetics of (OH, F, Cl)-bearing apatite, J. Biomed. Mater. Res., Part A 76 (2006) 753–764.
[27] D.L. Bish, J.E. Post, in: P.H. Ribbe (Ed.), Modern Powder Diffraction, Reviews in Mineralogy, vol. 20, Mineralogical Society of America, Washington, DC, 1989.
[28] S.N. Danilchenko, A.V. Koropov, I.Y. Protsenko, B. Sulkio-Cleff, L.F. Sukhodub, Thermal behavior of biogenic apatite crystals in bone: an X-ray diffraction study, Cryst. Res. Technol. 41 (2006) 268–275.
[29] P.F. Fewster, X-ray analysis of thin films and multilayers, Rep. Prog. Phys. 59 (1996) 1339.
[30] F.S. Wong, J.C. Elliott, Theoretical explanation of the relationship between backscattered electron and X-ray linear attenuation coefficients in calcified tissues, Scanning 19 (1997) 541–546.
[31] M. Todoh, S. Tadano, B. Giri, M. Nishimoto, Effect of gradual demineralization on the mineral fraction and mechanical properties of cortical bone, J. Biomech. Sci. Eng. 4 (2009) 230–238.
[32] S.N. Danilchenko, O.V. Kochenko, A.N. Kalinkevich, A.O. Stepanenko, Y.I. Zinchenko, P.S. Danylchenko, I.Y. Protsenko, Calibration of X-ray diffraction measurements for depth-selective structural analysis of two-layer samples, J. Nano- Electron. Phys. 13 (2021), 02037, https://doi.org/10.21272/jnep.13(2).02037.
[33] B.L. Henke, E.M. Gullikson, J.C. Davis, Atomic Data Nucl. Data Tables 54 (1993) 181. https://henke.lbl.gov/optical_constants/.
[34] S. Debnath, P. Predecki, R. Suryanarayanan, Use of glancing angle X-ray powder diffractometry to depth-profile phase transformations during dissolution of indomethacin and theophylline tablets, Pharm. Res. 21 (2004) 149–159.
[35] J. Liu, R.E. Saw, Y.H. Kiang, Calculation of effective penetration depth in X-ray diffraction for pharmaceutical solids, J. Pharmaceut. Sci. 99 (2010) 3807–3814.